Simulation de la rupture ductile : de la microstructure à la structure

Jacques Besson

Centre des Matériaux, Mines Paris, Paristech, CNRS UMR 7633

Outline

Micro-mechanisms of ductile failure

Mechanisms of ductile fracture

- The three stages of ductile fracture

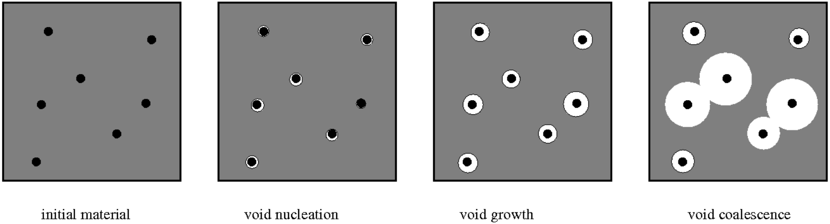

Mechanisms of ductile fracture : Nucleation

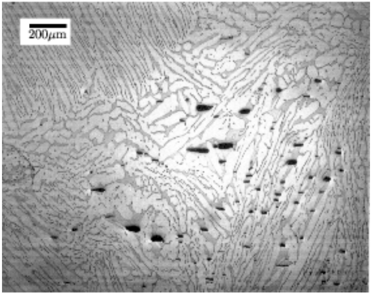

Duplex steel

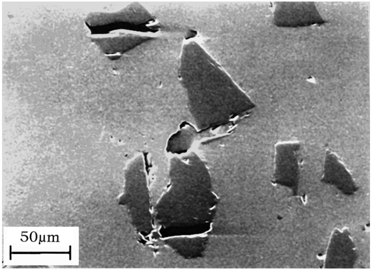

Al-Sic (coarse)

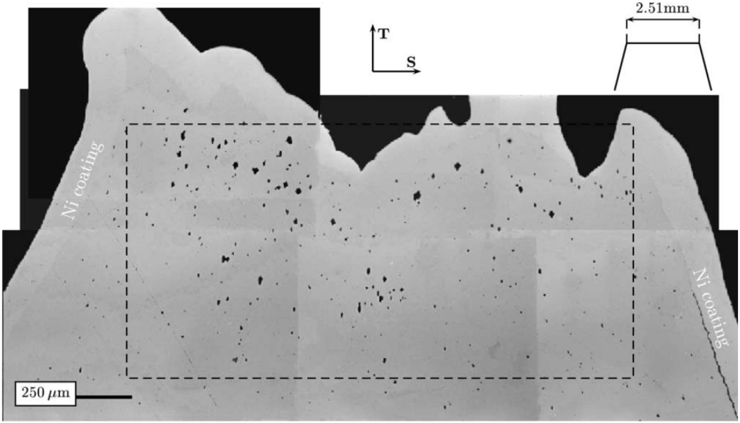

X52 line pipe steel

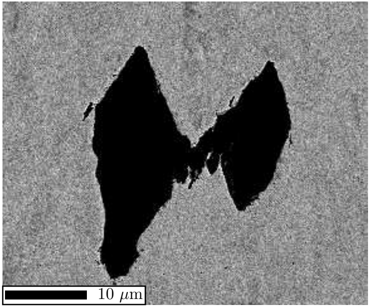

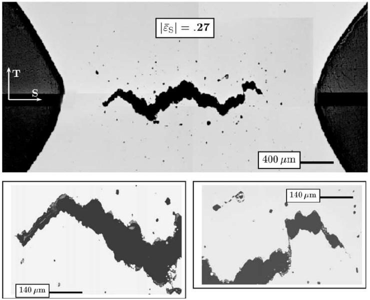

X52 line pipe steel

[Benzerga et al., 2004]

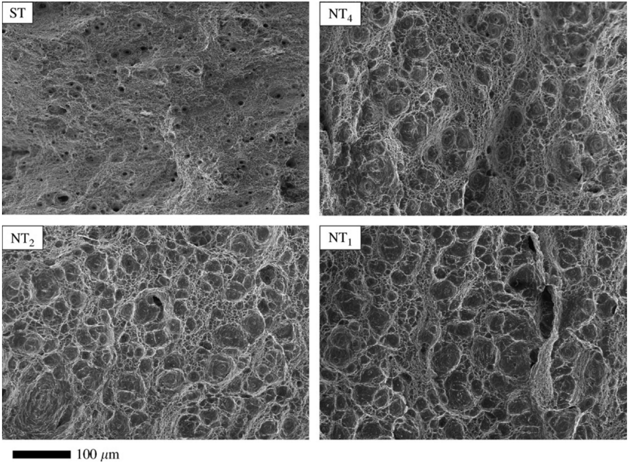

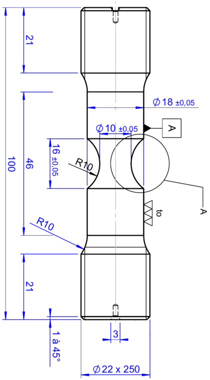

X100 line pipe steel

[Tanguy et al., 2008]

The Rice and Tracey model

The Rice and Tracey model (1969)

- Study of a single cavity within an infinite perfectly plastic medium (von Mises)

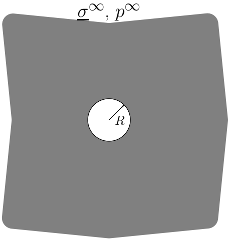

- Main result : evolution law for the void radius

$$\frac{\dot{R}}{R} = 0.283 \exp\left(\frac{3}{2}\frac{\sigma_m^{\infty}}{\sigma_{\text{eq}}^{\infty}}\right)\dot{p}^{\infty}$$

- With $\sigma_m = \sigma_{kk}/3$
- Role of both plastic strain p^{∞} and stress triaxiality $\sigma_m^{\infty}/\sigma_{\text{eq}}^{\infty}$

$$\tau(\underline{\sigma}) = \frac{\sigma_m}{\sigma_{\text{eq}}}$$

[Rice and Tracey, 1969]

The R&T model as a failure criterion

- The void growth rate is integrated over the load history :

$$\log(R/R_0) = \int_{\text{history}} dR/R = \int_{p_c}^{p} \alpha \exp(\beta\tau)\, dp$$

- Failure occurs when the void growth ration has reached a critical value which is assumed to be a material parameter

$$\frac{R}{R_0} = \left.\frac{R}{R_0}\right|_c$$

- The model simply represents the three stages of ductile rupture :

$$\begin{aligned}
\text{nucleation}: &\ p_c \\
\text{growth}: &\ \dot{R}/R = \alpha \exp(\beta\tau)\, \dot{p} \\
\text{coalescence}: &\ R/R_0 = R/R_0|_c
\end{aligned}$$

- The model is applied as a post-processing of an elasto-plastic calculation
- Crack advance can be modeled by removing elements for which $R/R_0 \geq R/R_0|_c$
- Main drawback : no coupling between plasticity and damage

[Marini et al., 1985]

- One considers two types of test specimens/structures

notched	cracked
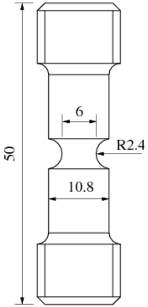	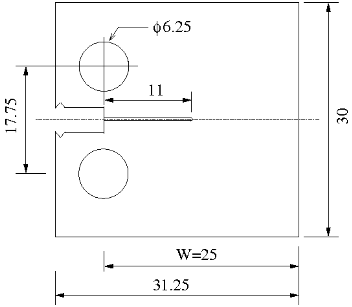

The R&T model as a failure criterion

- FE meshes

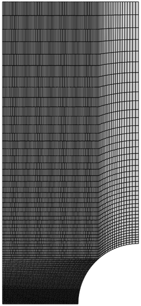

50μm

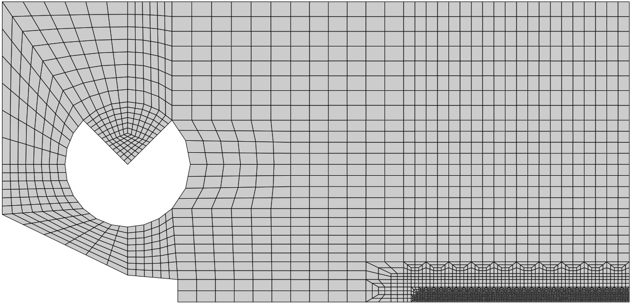

100μm

The R&T model damage indicator

- Simulation for different mesh sizes : 200, 100, 50 and 25μm.

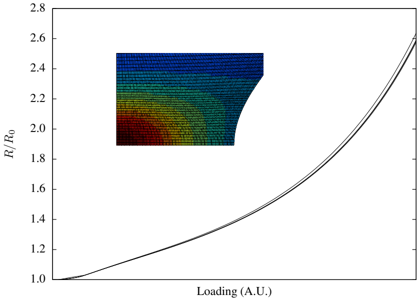

Notched

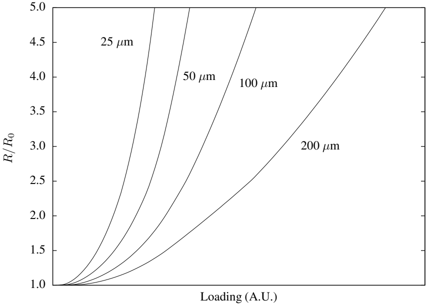

Cracked

- Very high stress/strain gradient at crack tip (HRR field)

$$\sigma_{ij} \propto 1/r^{\frac{1}{n+1}} \qquad \varepsilon_{ij} \propto 1/r^{\frac{n}{n+1}}$$

- Many models can be developed based on the same guidelines :

$$\dot{D} = \textsc{Function}\,(\text{stress state}, p)\ \dot{p}$$

- Failure $D = D_c$ $(= 1)$
- In particular, models now account for the role of the Lode parameter :

$$\mathcal{L} = \frac{27}{2} \frac{\det \underline{s}}{\sigma_{\mathrm{eq}}^3} \qquad -1 \leq \mathcal{L} \leq 1$$

- Experimental results indicate that ductility is reduced when $\mathcal{L} = 0$, *i.e.* shear/plane strain state . . . in particular at low triaxiality

[Defaisse et al., 2018]

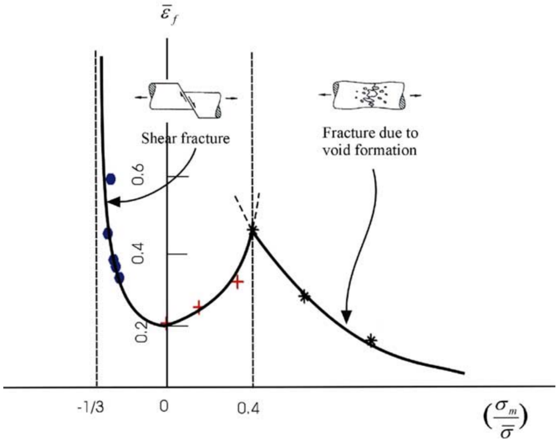

[Bao and Wierzbicki, 2005]

The Gurson model

The Gurson model (1977)

- Accounting for the coupling between plasticity and damage growth

$$f = \left(\frac{a}{b}\right)^3$$

$$V \propto b^3$$

$$V_m \propto b^3 - a^3$$

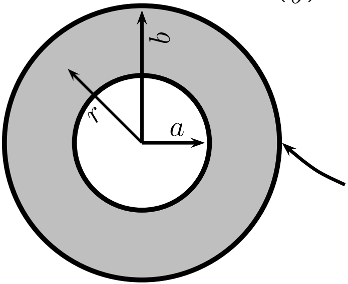

$\underline{\dot{E}}.\vec{x}$: imposed

- f : porosity ; damage variable

[Gurson, 1977]

The Gurson model : Hypothesis

- Rigid material, perfectly plastic (no work hardening)
- Spherical cavity
- Derived based on a micromechanical analysis (upper bound theory)
- Only one damage variable

➽ Results :

- Derivation of a plastic yield surface
- Plastic flow follows normality rule

- Yield surface :

$$\Phi = \frac{\sigma_{\text{eq}}^2}{\sigma_0^2} + 2f\cosh\left(\frac{1}{2}\frac{\sigma_{kk}}{\sigma_0}\right) - 1 - f^2 = 0$$

- σ_{eq} von Mises stress ; if $f = 0$ $\Phi \to$ von Mises
- $\sigma_{kk} = \text{trace}\underline{\sigma}$
- σ_0 matrix yield limit

- f is the only damage variable

$$f = \frac{V - V_m}{V} = 1 - \frac{V_m}{V}$$

where V_m is the matrix volume ; neglecting elastic deformation $V_m = \text{cte}$ so that :

$$\dot{f} = \frac{\dot{V}}{V} - \frac{V - V_m}{V^2}\dot{V} = \frac{V_m}{V}\frac{\dot{V}}{V} = (1-f)\frac{\dot{V}}{V} = (1-f)\text{trace}\,(\underline{\dot{\varepsilon}}) \simeq (1-f)\text{trace}\,(\underline{\dot{\varepsilon}}_p)$$

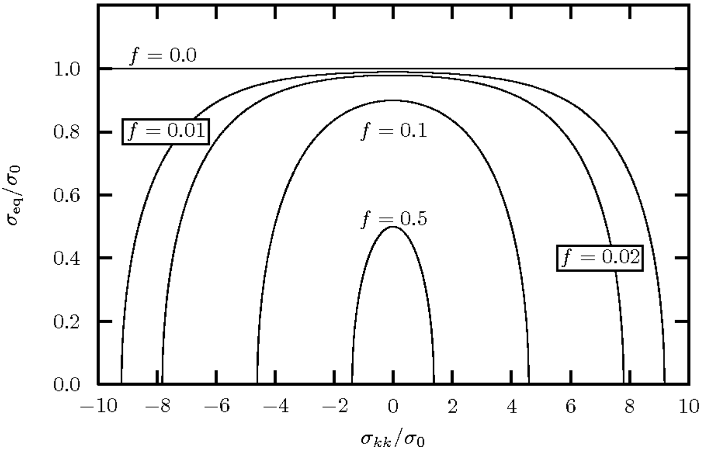
$f = 0.0$
$f = 0.01$
$f = 0.1$
$f = 0.5$
$f = 0.02$
1.0
0.8
0.6
0.4
0.2
0.0
σ_{eq}/σ_0
−10
−8
−6
−4
−2
0
2
4
6
8
10
σ_{kk}/σ_0

- Plastic flow using normality rule

$$\underline{\dot{\varepsilon}}_p = \dot{\lambda}\frac{\partial\Phi}{\partial\underline{\sigma}} = \dot{\lambda}\left[\frac{3}{\sigma_0^2}\underline{s} + \frac{f}{\sigma_0}\sinh\left(\frac{1}{2}\frac{\sigma_{kk}}{\sigma_0}\right)\underline{1}\right]$$

- Damage evolution : volume variation

$$\mathrm{trace}\left(\underline{\dot{\varepsilon}}_p\right) = \dot{\lambda}\frac{3f}{\sigma_0}\sinh\left(\frac{1}{2}\frac{\sigma_{kk}}{\sigma_0}\right) \neq 0$$

- Mass conservation (matrix) :$\dot{f} = (1-f)\mathrm{trace}\left(\underline{\dot{\varepsilon}}_p\right)$

! Damage rate is controlled by the definition of the yield surface ; no need to add an evolution law for damage.

- Dependence of damage rate on stress state

$$\sinh \approx \exp \qquad \sigma_0 \approx \sigma_{\mathrm{eq}} \qquad \text{Gurson shows similar trends as R\&T}$$

For high damage

$$\frac{1}{2}\frac{\sigma_{kk}}{\sigma_0} < \frac{1}{2}\frac{\sigma_{kk}}{\sigma_{\mathrm{eq}}}$$

- Rupture occurs when the stress state $\underline{\sigma} = \underline{0}$ lies on the yield surface
- Application to the Gurson model
  $\sigma_{\mathrm{eq}} = 0, \ \sigma_{kk} = 0$

$$
\begin{aligned}
\Phi &= \frac{0^2}{\sigma_0^2} + 2f\cosh\left(\frac{1}{2}\frac{0}{\sigma_0}\right) - 1 - f^2 \\
&= 2f\cosh(0) - 1 - f^2 \\
&= -(1-f)^2 = 0
\end{aligned}
$$

Rupture if $f = 1$

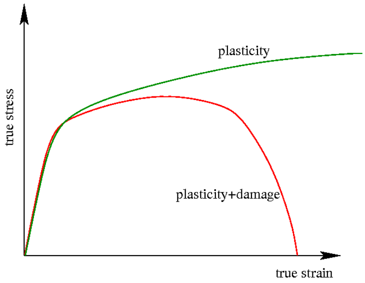

The Gurson model — summary

- The Gurson model has some interesting micromechanical basis to describe void growth and its interaction with plasticity
- Cavities are spherical
- it cannot model nucleation (voids are assumed to pre-exist)
- it cannot model coalescence and final rupture

➽ *ad hoc* phenomenological modifications of the model : the GTN model

The GTN model

The GTN model (Tvergaard+Needleman)

- Account for the elasto-plastic behaviour including isotropic hardening
- Better account for cavity growth

$$\Phi = \frac{\sigma_{\mathrm{eq}}^2}{\sigma_f^2} + 2q_1 f \cosh\left(\frac{q_2}{2}\frac{\sigma_{kk}}{\sigma_f}\right) - 1 - {q_1}^2 f^2 = 0$$

- σ_f matrix flow stress
- f : volume fraction of cavities in a reference stress state
  (elastic volume change is not damage)
- Plastic flow using normality : $\quad \underline{\dot{\varepsilon}}_p = \lambda \dfrac{\partial \Phi}{\partial \underline{\sigma}}$
- Damage growth : $\dot{f} = (1-f)\mathrm{trace}\underline{\dot{\varepsilon}}_p$
- Rupture for $f = 1/q_1$ (still to high)
- Usual values for q_1 and q_2 : $q_1 = 1.5$ and $q_2 = 1.0$
- Finite strain formulation

[Tvergaard and Needleman, 1984]

Definition of an equivalent scalar plastic strain

- σ_f function of p (isotropic hardening).
  Both σ_f and p are representative of the matrix
- Equality between microscopic plastic dissipation and macroscopic plastic dissipation (HEM)

$$\begin{array}{rcl} (1-f)\dot{p}\sigma_\star & = & \underline{\dot{\varepsilon}_p} : \underline{\sigma} \\ \text{micro} & = & \text{macro} \end{array}$$

The equivalent scalar plastic strain is not equal to the von Mises plastic strain

$$\dot{p} \neq \sqrt{\frac{2}{3}\underline{\dot{\varepsilon}_p} : \underline{\dot{\varepsilon}_p}} \neq \sqrt{\frac{2}{3}\underline{\dot{\varepsilon}'_p} : \underline{\dot{\varepsilon}'_p}}$$

- Important damage process : new cavities appear

$$\dot{f} = (1 - f)\mathrm{trace}\underline{\dot{\varepsilon}}_p + \dot{f}_n$$

- $(1 - f)\mathrm{trace}\underline{\dot{\varepsilon}}_p$: void growth
- $\dot{f}_n$: nucleation
- Strain controlled nucleation

$$\dot{f}_n = A_n(\ldots)\dot{p}$$

- (stress controlled nucleation)

The GTN model : Strain controlled nucleation

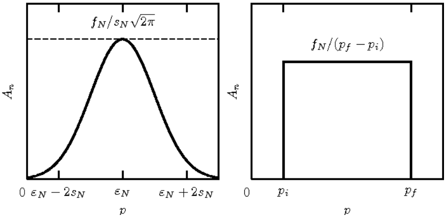

- Phenomenological approach

$$\dot{f}_n = A_n(\dots)\dot{p}$$

- A_n can be adjusted on macroscopic or microscopic tests (many fitting parameters)
- Example [Chu and Needleman, 1980]

$$A_n = \frac{f_N}{\sqrt{2\pi}s_N}\exp\left(-\frac{(p-\varepsilon_N)^2}{2{s_N}^2}\right)$$

- One often (too often) finds in the literature :

$$\varepsilon_N = 0.3 \quad \text{et} \quad s_N = 0.1$$

- A_n may depend on the stress state (in particular on the stress triaxiality ratio)
- Some rules :
  —Experimentally determine if nucleation takes place
  — Try to experimentally identify nucleation parameters

- Define an effective porosity $f_\star$ to take into account coalescence

$$\Phi = \frac{\sigma_{\mathrm{eq}}^2}{\sigma_f^2} + 2 q_1 f_\star \cosh\left(\frac{q_2}{2}\frac{\sigma_{kk}}{\sigma_f}\right) - 1 - q_1^2 {f_\star}^2 = 0$$

- Simple form $f_\star$

$$f_\star = \begin{cases} f & \text{if } f < f_c \\ f_c + \dfrac{\frac{1}{q_1} - f_c}{f_R - f_c}(f - f_c) & \text{otherwise} \end{cases}$$

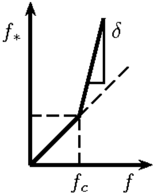

- Rupture : $f_\star = 1/q_1$ or $f = f_R$

The GTN model : Main result of the 1984 paper

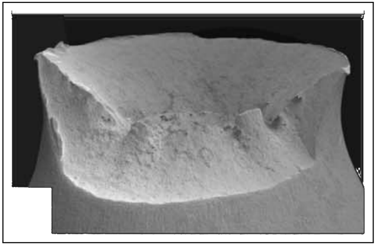

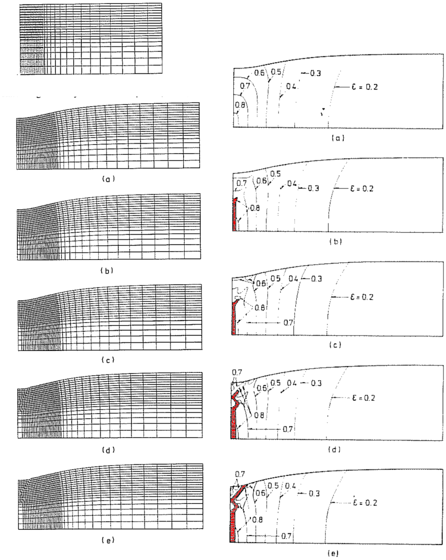
(a)
(b)
(c)
(d)
(e)
0.6
0.5
0.3
0.7
0.4
0.8
ε = 0.2

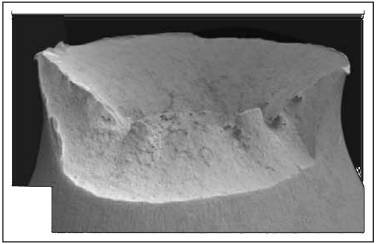

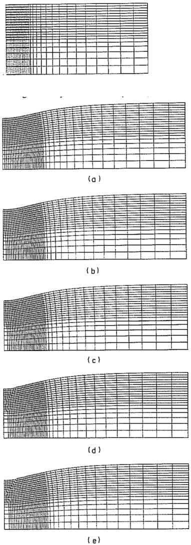

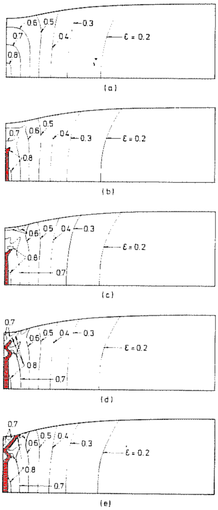

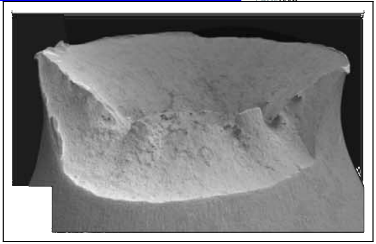

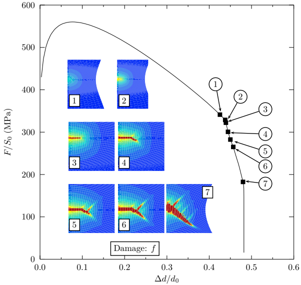

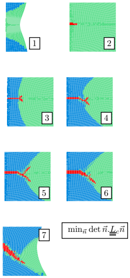

[Besson et al., 2001]

Extensions of the Gurson–Tvergaard–Needleman model

Extensions of the GTN model : Viscosity

- Case of the rate dependent materials
- $\sigma_f(p) \to \sigma_f(p, \dot{p})$
- This simple modification is valid for “weakly” rate dependent materials
- Example : Charpy impact test

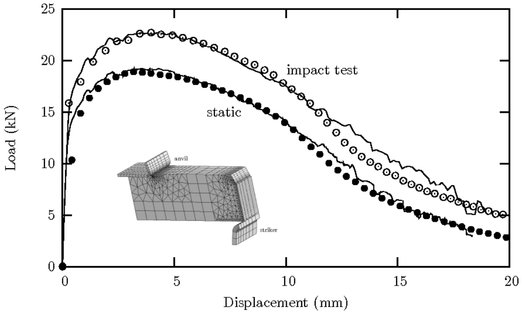

[Tanguy et al., 2008]

- The behavior of the undamaged materials is such that

$$\dot{p} = \dot{p}_0 \left(\frac{\sigma_{\mathrm{eq}}}{\sigma_0}\right)^n \qquad \text{or} \qquad \sigma_{\mathrm{eq}} = \sigma_0 \left(\frac{\dot{p}}{\dot{p}_0}\right)^m = \sigma_f(\dot{p}) \qquad m = 1/n$$

- A (possible) corresponding yield function of the porous material is :

$$\Phi = \frac{\sigma_{\mathrm{eq}}^2}{\sigma_f^2} + q_1 f_\star \left[h_m\left(\frac{1}{2} q_2 \frac{\sigma_{kk}}{\sigma_f}\right) + \frac{1-m}{1+m} \frac{1}{h_m\left(\frac{1}{2} q_2 \frac{\sigma_{kk}}{\sigma_f}\right)} \right] - 1 - q_1^2 \frac{1-m}{1+m} f_\star^2 \equiv 0$$

with $m = 1/n$ and

$$h_m(x) = \left(1 + m x^{1+m}\right)^{1/m}$$

- Limit cases : $m \to 0$: GTN model, $m = 1$: “ellipic model” :

$$\Phi = \sigma_{\mathrm{eq}}^2 + \frac{1}{4} q_1 q_2^2 \sigma_{kk}^2 - (1 - q_1 f_\star) \sigma_f^2$$

[Leblond et al., 1994]

- Anisotropic plastic flow — Anisotropic plastic yielding (X100 line pipe steel)

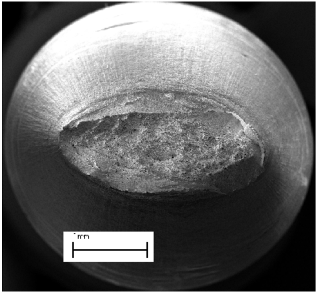

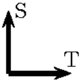

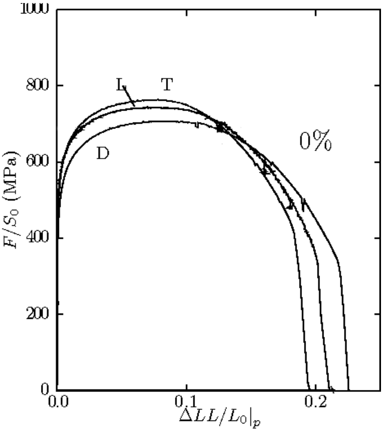

[Shinohara et al., 2016]

- Extension of the GTN in the case of a matrix obeying the Hill (1948) yield criterion :

$$\sigma_H = \sqrt{\frac{3}{2}\left(h_{11}s_{11}^2 + h_{22}s_{22}^2 + h_{33}s_{33}^2 + 2h_{12}s_{12}^2 + 2h_{23}s_{23}^2 + 2h_{31}s_{31}^2\right)} = \sigma_f(p)$$

- Intuition [Brunet and Morestin, 2001, Rivalin et al., 2000]

$$\Phi = \left(\frac{\sigma_H}{\sigma_f}\right)^2 + 2q_1 f_\star \cosh\left(\frac{q_2}{2}\frac{\sigma_{kk}}{\sigma_f}\right) - 1q_1^2 f_\star^2 = 0$$

- valid as the Gurson derivation applied to a Hill matrix leads to [Benzerga and Besson, 2001] :

$$\Phi = \left(\frac{\sigma_H}{\sigma_0}\right)^2 + 2f\cosh\left(\frac{1}{h}\frac{\sigma_{kk}}{\sigma_0}\right) - 1 - f^2 = 0 \quad \text{with } h = \sqrt{\frac{8}{5}\frac{h_{11}+h_{22}+h_{33}}{h_{11}h_{22}+h_{11}h_3+h_{22}h_{33}} + \frac{4}{5}\left(\frac{1}{h_{12}}+\frac{1}{h_{23}}+\frac{1}{h_{31}}\right)}$$

- when $f \ll 1$, $\sigma_H \approx \sigma_f$ so that void growth is controlled by $\frac{1}{3}\sigma_{kk}/\sigma_H$; this calls for the definition of an appropriate triaxiality ratio [Shinohara et al., 2016] :

$$\tau_H = \frac{1}{3}\frac{\sigma_{kk}}{\sigma_H}$$

- ☺ Extension to any stress measure [Bron and Besson, 2006]

$$\Phi = \left(\frac{\text{Your stress measure}}{\sigma_f}\right)^2 + 2q_1 f_\star \cosh\left(\frac{q_2}{2}\frac{\sigma_{kk}}{\sigma_f}\right) - 1 - q_1^2 f_\star^2 = 0$$

Extensions of the GTN model : Void shape

- Inclusions and therefore voids may be elongated (prolate) or flat (oblate)
- How does this affect void growth ?
- Example : X52 steel containing elongated MnS inclusions

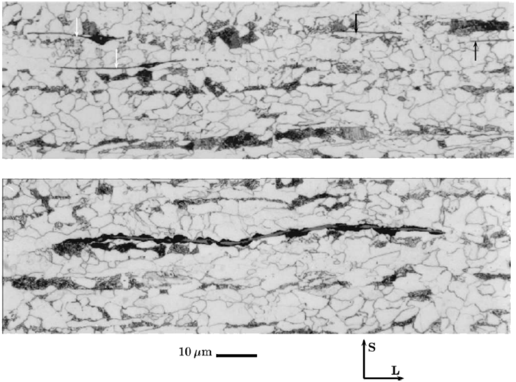

[Benzerga et al., 2004]

The Gologanu–Leblond–Devaux model

- Two cofocal axisymmetric ellipsoids (void+cell)

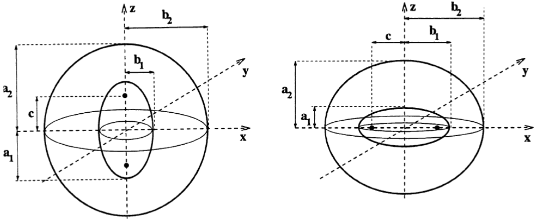

elongated (prolate)

flat (oblate)

- One extra material variable :

$$S = \log\left(\frac{a_1}{b_1}\right) \qquad \begin{cases} S > 0 & \text{elongated voids} \\ S = 0 & \text{spherical voids / i.e. Gurson} \\ S < 0 & \text{flat voids} \end{cases}$$

- Void symmetry axis : $\vec{e}_z$

[Gologanu et al., 1993, Gologanu et al., 1994]

Application of the GLD model

- Contour plots of $w = \exp S$ in the case of a notched bar for elongated and flat cavities

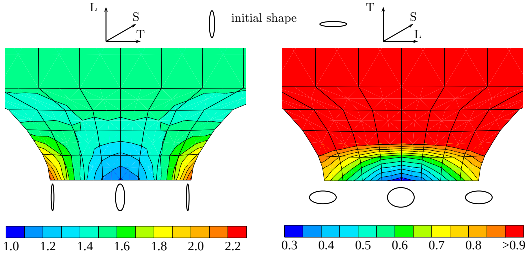

Two drawbacks of the model
- In practice, axisymmetric cavities do not remain axisymmetric. . .and two shape factors are needed
- there is no relative rotation of the cavity axis with respect to the material

☺ Solved : [Danas and Aravas, 2012, Madou and Leblond, 2012a, Madou and Leblond, 2012b, Cao et al., 2015]

- Thomason analysis [Thomason, 1985b, Thomason, 1985a] : two possible deformation modes :

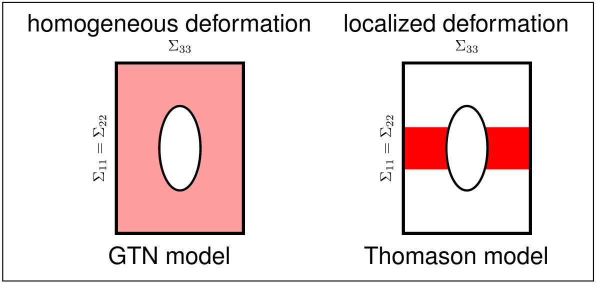

- Condition for coalescence

$$\pi L^2 \Sigma_{33} = \pi (L^2 - R_x^2) \mathcal{C}_f \sigma_f$$

with

$$C_f = 0.1 \left(\frac{R_z}{L - R_x} \right)^{-2} + 1.2 \sqrt{L/R_x}$$

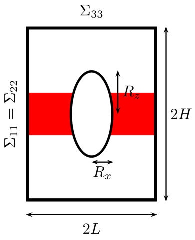

$$\dot{\underline{\varepsilon}}_p \propto \begin{pmatrix} 0 & 0 & 0 \\ 0 & 0 & 0 \\ 0 & 0 & 1 \end{pmatrix}$$

Using the Thomason model

- Use the Thomason model to **detect** coalescence ; $f_c = f$ at the onset of coalescence ; use the GTN model with the $f_\star$ function with the evaluated value for f_c [Zhang et al., 2000].
- Search for a coalescence direction over all directions, or directions corresponding to the maximum eigenvalue of $\underline{\sigma}$, $\underline{\varepsilon}_p$ or $\underline{\dot{\varepsilon}}_p$
- Use a simplified version based on yield surface (multi-surface model) [Besson, 2009]

$$\Phi = \frac{2}{3}\sigma_{\mathrm{eq}} + \frac{1}{3}|\sigma_{kk}| - C_{\mathrm{th}}\sigma_f = 0$$

- Very little use of the model in FE simulations up to now
- Many extensions . . . : hardening [Pardoen and Hutchinson, 2000], shear [Torki et al., 2015], very flat voids [Hure and Barrioz, 2016],. . ..

Example GTN+Thomason

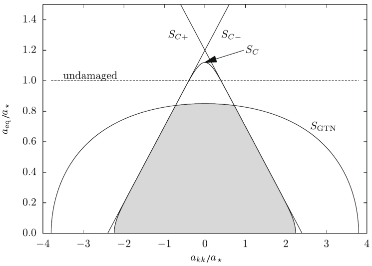

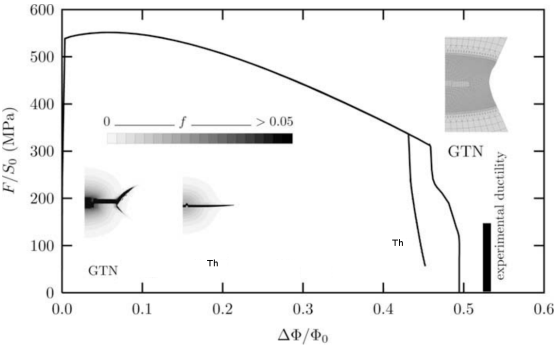

Low triaxiality shear failure

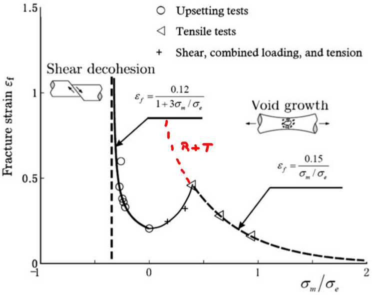

[Nahshon and Hutchinson, 2008,

Bao and Wierzbicki, 2004, Mae et al., 2007]

- Low triaxiality ($\tau < 1$) and Lode parameter ($\mathcal{L} = \frac{27}{2} \det \underline{s}/\sigma_{\mathrm{eq}}^3$) close to 0 : lower ductilities compared to prediction made from high triaxiality data.
- Additional damage given has :

$$\dot{f}_{\mathrm{sh}} = k_w f w(\mathcal{L}) \underline{s} : \dot{\underline{\varepsilon}}_p / \overline{\sigma}$$

[Nahshon and Hutchinson, 2008]

- The effect of the Lode parameter is validated by unit cell calculations :

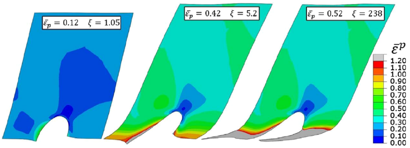

[Dunand and Mohr, 2014]

- Nano-voids are created due to irradiation (304 and 306 SS).

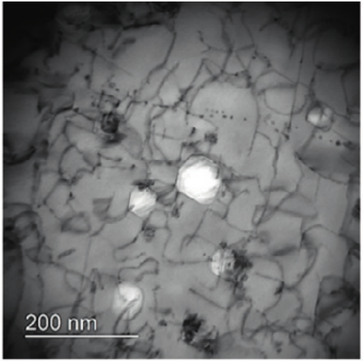

[Gallican and Hure, 2017]

- A yield function can be defined for each slip system s as [Han et al., 2013] :

$$\left(\frac{\tau_s^2}{\tau_{cs}^2}+\alpha\frac{2}{45}\frac{\sigma_{\mathrm{eq}}^2}{\tau_{cs}^2}\right)+2q_1 f\cosh\left(q_2\sqrt{\frac{3}{20}}\frac{\sigma_m}{\tau_{cs}}\right)-1-q_1^2f^2=0$$

- Can be fitted on unit cell simulations
- Alternative solutions in [Paux et al., 2015, Mbiakop et al., 2015], coalescence in [Gallican and Hure, 2017].

What about nucleation ?

- Growth and coalescence = plasticity (continuum mechanics)

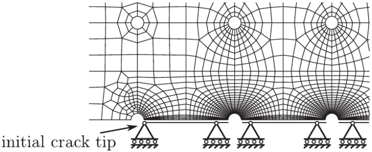

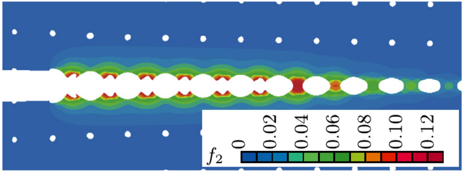

[Hütter et al., 2014]

- Modeling of nucleation remains essentially phenomenological
- Evaluation of stresses in the particles leading to damage nucleation [Beremin, 1981] :

$$\sigma_I^p = \Sigma_I + k(p, \text{shape})(\Sigma_{\text{eq}} - \sigma_0)$$

- Use estimates of σ_I^p together with a probabilistic distribution of the inclusion failure stress (*e.g.* Weibull like) to derive the nucleation kinetics.
- *In situ* informations obtained by X-ray tomography can help.
- This approach is valid for sizes equal to $\approx 1\mu$m and above ... but probably not for nanometric particles.

What about nucleation ?

- Simulation of particle cracking and void growth

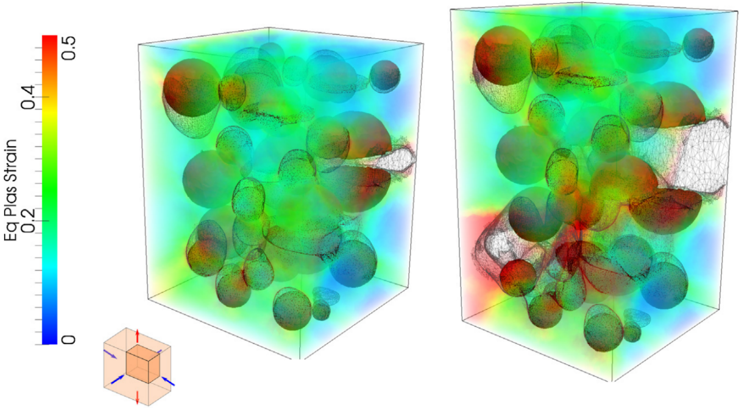

[Shakoor et al., 2018]

Strain and damage localization

Strain and damage localization

- Damage leads to cracking : *i.e.* localized damage and strain
- Condition for localization [Rice, 1976, Rice, 1980, Rudnicki and Rice, 1975, Needleman and Rice, 1978]

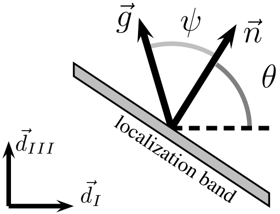

- One assumes an elasto-plastic behavior (rate independent) so that :

$$\underset{\sim}{\dot{\sigma}} = \underset{\approx}{\mathcal{L}}_t : \underset{\sim}{D}$$

- Jum across the band

$$[\![\underset{\sim}{D}]\!]_{\text{band}} \propto \frac{1}{2}(\vec{g} \otimes \vec{n} + \vec{n} \otimes \vec{g})$$

- Equilibrium

$$[\![\underset{\sim}{\dot{\sigma}}]\!]_{\text{band}} . \vec{n} = \vec{0}$$

- the equilibrium equation is rewritten as :

$$[\![\dot{\sigma}]\!] .\vec{n} = \vec{0} \;\Rightarrow\; \underset{\approx}{\mathcal{L}}_t : [\![\dot{\varepsilon}]\!] .\vec{n} = \vec{0} \;\Rightarrow\; \underset{\approx}{\mathcal{L}}_t : (\vec{g} \otimes \vec{n}).\vec{n} = \vec{0}$$

or using indexes :

$$L_{ijkl} g_k n_l n_j = n_j L_{ijkl} n_l g_k = n_j L_{\color{red}{ji}kl} n_l g_k = 0_i$$

or introducing a specific second order tensor $\underset{\sim}{A}$

$$A_{ik} g_k = 0_i \text{ with } A_{ik} = n_j L_{jikl} n_l$$

- A_{ik} represents a second order tensor $\underset{\sim}{A}$ and the previous relation can be rewritten as :

$$\underset{\sim}{A}.\vec{g} = \left(\vec{n}.\underset{\approx}{\mathcal{L}}.\vec{n}\right).\vec{g} = \vec{0}$$

so that :

(i) $\vec{g} = \vec{0}$ (i.e. no jump)

(ii) $\boxed{\det\left(\vec{n}.\underset{\approx}{\mathcal{L}}.\vec{n}\right) = 0}$ and $\underset{\sim}{g}$ is the eigenvector corresponding to the null eigenvalue.

(iii) The band thickness is not predicted

- Localization indicator

$$I_L = \min_{\vec{n},\, ||\vec{n}||=1} \det \vec{n}.\underline{\underline{\mathcal{L}}}_t.\vec{n}$$

- Localization becomes possible if :

$$I_L < 0$$

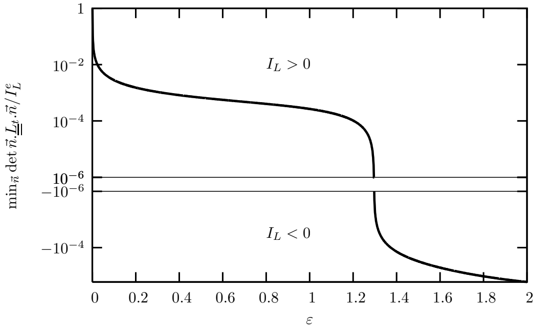

[Billardon and Doghri, 1989, Besson et al., 2001]

Analysis of cup–cone formation

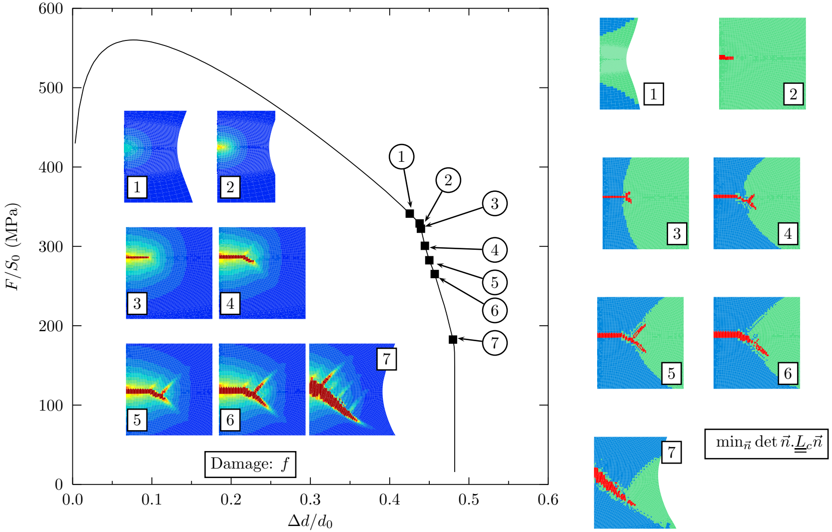

Simulation using the finite element method

- GTN model with the following parameters

f_0	q_1	q_2	f_c	f_R	$\sigma_F(p)$ (MPa)
0.001	1.47	1.05	0.05	0.25	$510 + 295(1 - \exp(-9.6p))$

  corresponding to a modern construction steel
- No nucleation (rupture at high stress triaxiality)
- Identification of material parameters is still a open problem

- Simulations : plane strain, bi-linear 4-node elements, B-bar method (pressure control)
- Element removal technique
- Various mesh sizes

Simulation: NT specimen

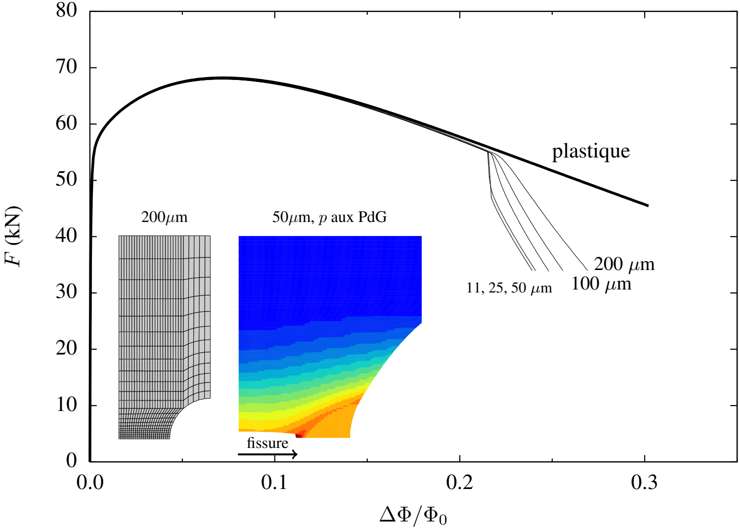

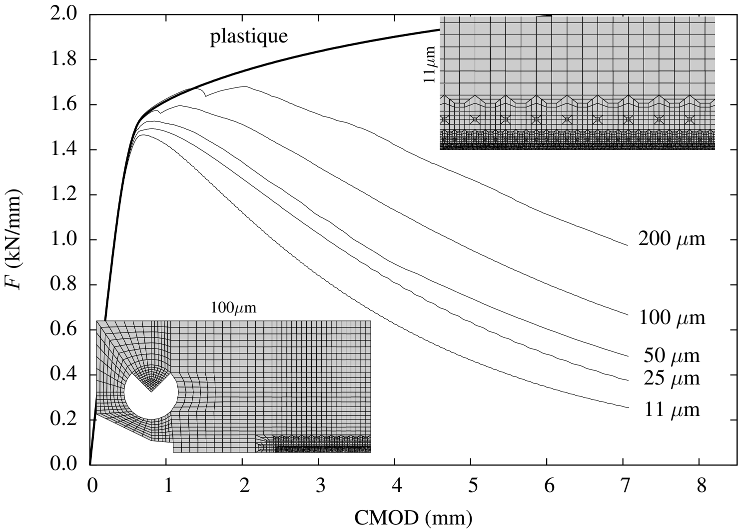
plastique
11μm
100μm
200 μm
100 μm
50 μm
25 μm
11 μm
F (kN/mm)
CMOD (mm)
0.0
0.2
0.4
0.6
0.8
1.0
1.2
1.4
1.6
1.8
2.0
0
1
2
3
4
5
6
7
8

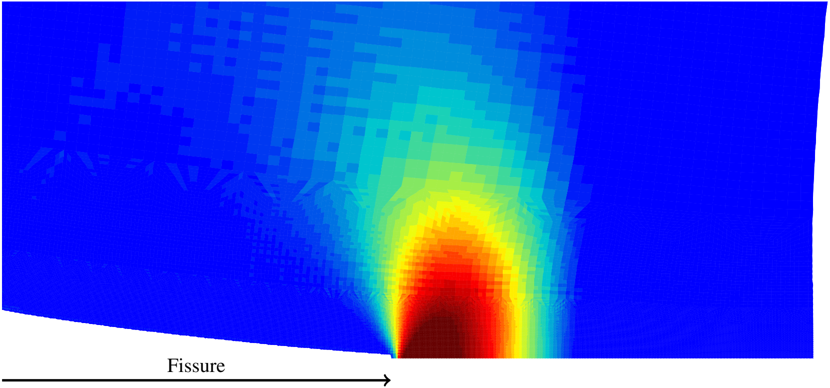

Contrainte d'ouverture (bleu : $\sigma_{22} < 0$,MPa rouge : $\sigma_{22} > 1500$ MPa

Simulation: Need for a material length

- Models provide a volumic fracture energy : w_0 J.m^{-3}
- This energy describes well crack initiation in an uncracked structure
- Fracture is characterized by a surfacic fracture energy : γ_0 J.m^{-2}
- The ratio

$$\Lambda = \gamma_0 / w_0$$

  is a material length
- The material can be "seen" as an arrangement of material cells

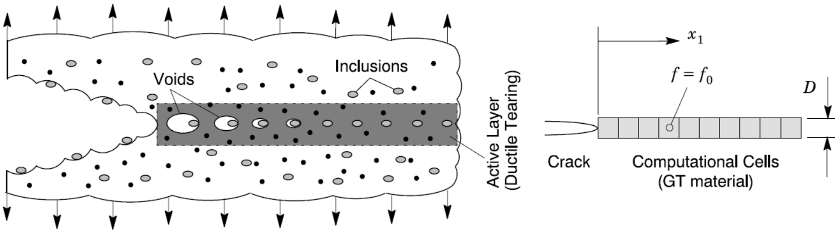

[Xia and Shih, 1995, Xia et al., 1995, Ruggieri et al., 1996, Besson et al., 2013]

Simulation: Need for a material length
A first solution

- Use a fixed mesh type : interpolation, size, aspect ratio, orientation
- This solution is very often used (sometimes implicitly. . .)
- Allows transfer to one geometry to another
- Failed elements can be removed from the calculation

☺ Easy to use method

☹ Element size is used to (i) discretized the geometry, (ii) determine the fracture energy γ_0

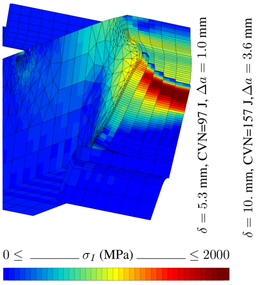

[Tanguy et al., 2005]

Simulation: Need for a material length
A much better solution !

- Use enhanced models integrating material internal lengths (so called “non local” models).
- No mesh size dependence

[Zhang et al., 2018, Aldakheel et al., 2018, Enakoutsa et al., 2007, Mediavilla et al., 2006, Feld-Payet et al., 2011]

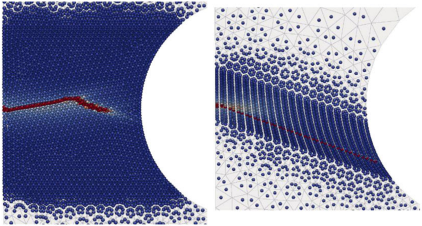

standard

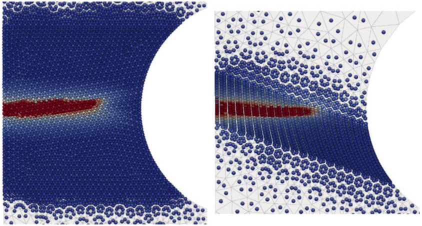

with material length

(Zhang, 2018)

- **Voir exposé de Éric Lorentz**

- Flat to slant transition in a steel plate [Besson et al., 2013]

- Geometry

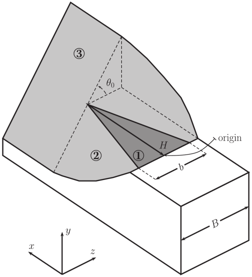

- Mesh design

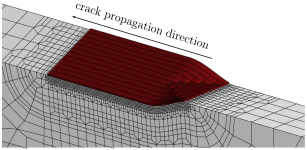

- Analysis of crack propagation depending on the **assumed** tilt angle

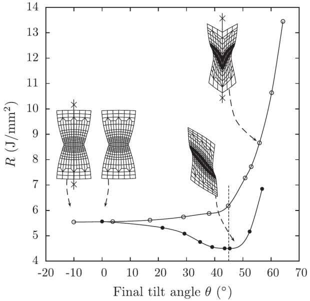

- Full size test on welded pipe (girth weld)

- Weld

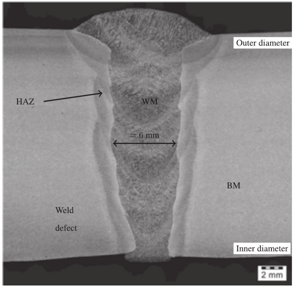

- Crack in the weld metal

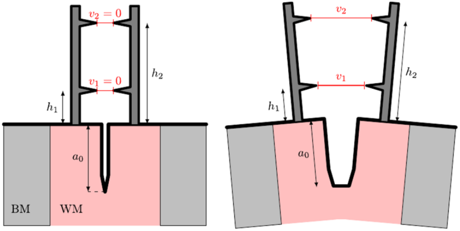

Initial state　　Deformed state

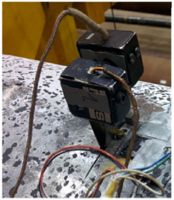

Clips mounted on the pipe

Simulation: Failure of a welded pipe (II)

- Material characterization : (BM) plasticity, (WM) plasticity and failure

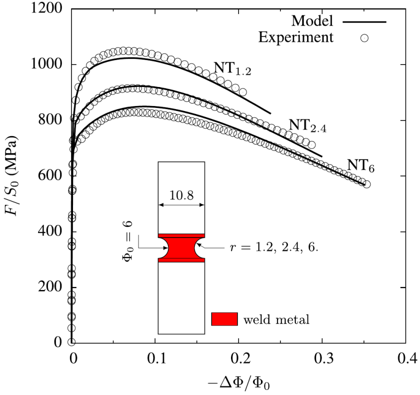

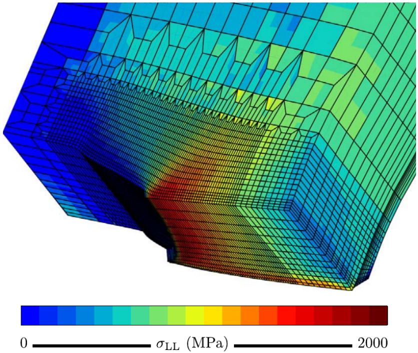

- Testing — Load displacement curve

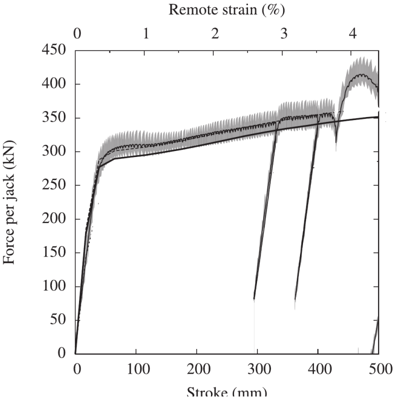

- Mesh design — CMOD and crack advance

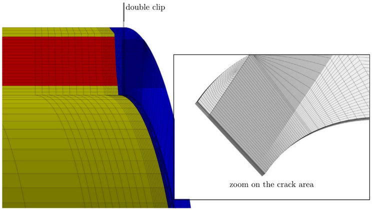

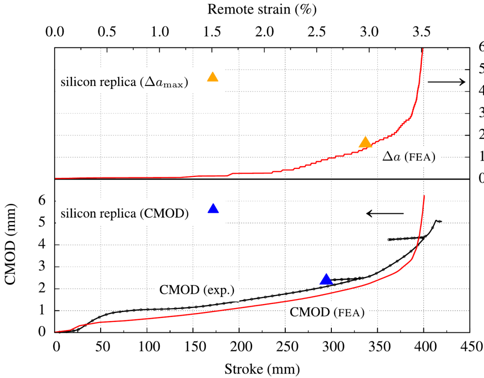

- Mesh design — CMOD and crack advance

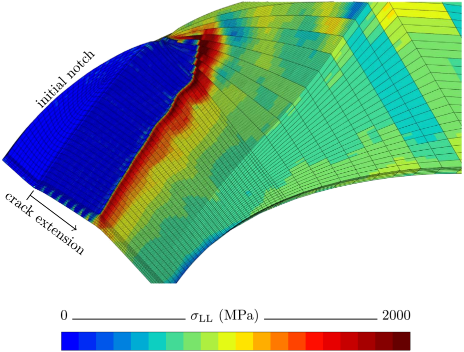

- Simulation used to better interpret full size test . . . and possible help the design of such tests

[Soret et al., 2017]

Conclusions

Conclusions

- Models for ductile rupture : many extensions to growth and coalescence of the seminal work of Gurson and Tvergaard—Needleman
- Much less developments concerning void nucleation from inclusions
- Applicability of the models (mainly GTN) to the simulation of specimens and structures
- Dealing with strain/damage localization and damage to crack transition is still a problem
- One possible solution is the use of continuum models with internal lengths
- . . . but many other solutions exist (CZM, XFEM+CZM, Thick Level set, Phase field, explicit introduction of discontinuities inside elements . . .)

- Flat to slant transition in an aluminum alloy

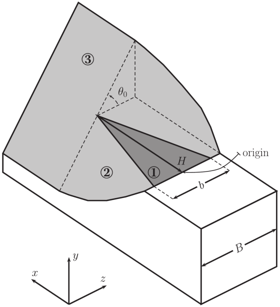

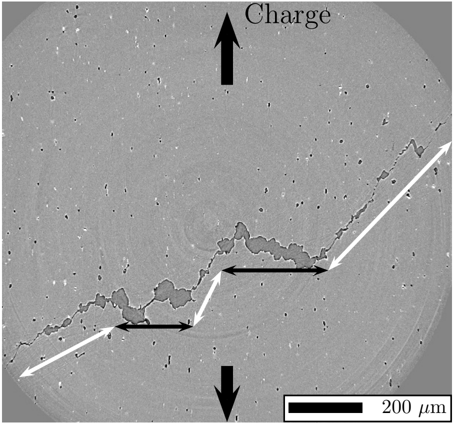

- **Model :** anisotropy, nucleation, growth, coalescence (internal necking and void sheeting)
- **Simulation :** Crack path change, full 3D, possible two length scales

Conclusions: Appel

- 2004 : Ecole d'été CNRS à Roscoff
- MEALOR : Mécanique de l'Endommagement et Approche LOcale de la Rupture !

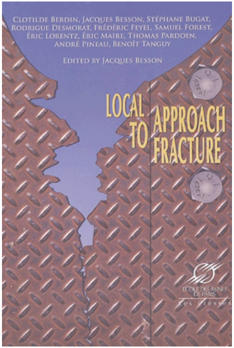

- Volontaire(s)
- Relancer une école
- Coordonner une nouvelle version du livre

- ESIS : European Structural Integrity Society
- Site : `http://www.esisweb.org`
- J. Besson avec T. Palin-Luc : représentants pour la France
- Technical committee on “Numerical methods for fracture” (TC8)
  - Une réunion par an
  - Numéros spéciaux pour **Engineering Fracture Mechanics**
- Contact : `jacques.besson@mines-paristech.fr`

Bibliography

Aldakheel, F., Wriggers, P., and Miehe, C. (2018).
A modified gurson-type plasticity model at finite strains : formulation, numerical analysis and phase-field coupling.
Computational Mechanics, 62(4) :815–833.

Bao, Y. and Wierzbicki, T. (2004).
On fracture locus in the equivalent strain and stress triaxiality space.
Int. J. Mech. Sci., 46(1) :81–98.

Bao, Y. and Wierzbicki, T. (2005).
On the cut-off value of negative triaxiality for fracture.
Eng. Fract. Mech., 72 :1049–1069.

Benzerga, A. and Besson, J. (2001).
Plastic potentials for anisotropic porous solids.
Eur. J. Mech./A, 20A(3) :397–434.

Benzerga, A., Besson, J., and Pineau, A. (2004).
Anisotropic ductile fracture Part I : experiments.
Acta Mater., 52 :4623–4638.

Beremin, F. M. (1981).
Cavity formation from inclusions in ductile fracture of A508 steel.
Met. Trans., 12A :723–731.

Besson, J. (2009).

Damage of ductile materials deforming under multiple plastic or viscoplastic mechanisms.
Int. J. Plasticity, 25 :2204–2221.

Besson, J., McCowan, C., and Drexler, E. (2013).
Modeling flat to slant fracture transition using the computational cell methodology.
Eng. Fract. Mech., 104 :80–95.

Besson, J., Steglich, D., and Brocks, W. (2001).
Modeling of crack growth in round bars and plane strain specimens.
Int. J. Solids Structures, 38(46–47) :8259–8284.

Billardon, R. and Doghri, I. (1989).
Prediction of macro-crack initiation by damage localization.
C. R. Acad. Sci. Paris, 308(Série II) :347–352.

Bron, F. and Besson, J. (2006).
Simulation of the ductile tearing for two grades of 2024 aluminum alloy thin sheets.
Eng. Fract. Mech., 73 :1531–1552.

Brunet, M. and Morestin, F. (2001).
Experimental and analytical necking studies of anisotropic sheet metals.
J. Mater. Processing Technol., 112 :214–226.

Cao, T., Maziere, M., Danas, K., and Besson, J. (2015).
A model for ductile damage prediction at low stress triaxialities incorporating void shape change and void rotation.
Int. J. Solids Structures, 63 :240–263.

Chu, C. and Needleman, A. (1980).
Void nucleation effects in biaxially stretched sheets.
J. Engng Mater. Technol., 102 :249–256.

Danas, K. and Aravas, N. (2012).
Numerical modeling of elasto-plastic porous materials with void shape effects at finite deformations.
Composites Part B : Engineering, 43(6) :2544 – 2559.

Defaisse, C., Mazière, M., Marcin, L., and Besson, J. (2018).
Ductile fracture of an ultra-high strength steel under low to moderate stress triaxiality.
Eng. Fract. Mech., 194 :301–318.

Dunand, M. and Mohr, D. (2014).
Effect of lode parameter on plastic flow localization after proportional loading at low stress triaxialities.
J. Mech. Phys. Solids, 66 :133–153.

Enakoutsa, K., Leblond, J., and Perrin, G. (2007).
Numerical implementation and assessment of a phenomenological nonlocal model of ductile rupture.
Comp. Meth. Appl. Mech. Engng, 196(13-16) :1946–1957.

Feld-Payet, S., Feyel, F., and Besson, J. (2011).
Finite element analysis of damage in ductile structures using a nonlocal model combined with a three-field formulation.
Int. J. Damage Mech., 20 :655–680.

Gallican, V. and Hure, J. (2017).
Anisotropic coalescence criterion for nanoporous materials.
J. Mech. Phys. Solids, 108 :30–48.

Gologanu, M., Leblond, J., and Devaux, J. (1993).
Approximate models for ductile metals containing non–spherical voids — case of axisymmetric prolate ellipsoidal cavities.
J. Mech. Phys. Solids, 41(11) :1723–1754.

Gologanu, M., Leblond, J., and Devaux, J. (1994).
Approximate models for ductile metals containing non–spherical voids — case of axisymmetric oblate ellipsoidal cavities.
J. Engng Mater. Technol., 116 :290–297.

Gurson, A. L. (1977).
Continuum theory of ductile rupture by void nucleation and growth : Part I— Yield criteria and flow rules for porous ductile media.
J. Engng Mater. Technol., 99 :2–15.

Han, X., Besson, J., Forest, S., Tanguy, B., and Bugat, S. (2013).
A yield function for single crystals containing voids.
Int. J. Solids Structures, 50 :2115–2131.

Hure, J. and Barrioz, P.-O. (2016).
Theoretical estimates for flat voids coalescence by internal necking.
Eur. J. Mech./A, 60 :217–226.

Hütter, G., Zybell, L., and Kuna, M. (2014).
Size effects due to secondary voids during ductile crack propagation.
Int. J. Solids Structures, 51 :839–847.

Leblond, J., Perrin, G., and Suquet, P. (1994).
Exact results and approximate models for porous viscoplastic solids.
Int. J. Plasticity, 10(3) :213–235.

Madou, K. and Leblond, J. (2012a).
A gurson-type criterion for porous solids containing arbitrary ellipsoidal voids — i : Limit-analysis of some representative cell.
J. Mech. Phys. Solids, 60 :1020–1036.

Madou, K. and Leblond, J. (2012b).
A gurson-type criterion for porous solids containing arbitrary ellipsoidal voids — ii : Determination of the yield criterion parameters.
J. Mech. Phys. Solids, 60 :1037–1058.

Mae, H., Teng, X., Bai, Y., and Wierzbicki, T. (2007).
Calibration of ductile fracture properties of a cast aluminum alloy.
Mater. Sci. Engng A, 459(1-2) :156–166.

Marini, B., Mudry, F., and Pineau, A. (1985).
Experimental study of cavity growth in ductile rupture.
Eng. Fract. Mech., 22(6) :989–996.

Mbiakop, A., Constantinescu, A., and Danas, K. (2015).
An analytical model for porous single crystals with ellipsoidal voids.
J. Mech. Phys. Solids, 84 :436–467.

Mediavilla, J., Peerlings, R., and Geers, M. (2006).
Discrete crack modelling of ductile fracture driven by non-local softening plasticity.
Int. J. Numer. Meth. Engng, 66(4) :661–688.

Nahshon, K. and Hutchinson, J. (2008).
Modification of the Gurson model for shear failure.
Eur. J. Mech./A, 27A :1–17.

Needleman, A. and Rice, J. (1978).
Limits to ductility set by plastic flow localization.
In D.P. Koistinen, e., editor, *Mechanics of Sheet Metal Forming*, pages 237–267. Plenum Publishing Corporation.

Pardoen, T. and Hutchinson, J. (2000).
An extended model for void growth and coalescence.
J. Mech. Phys. Solids, 48(12) :2467–2512.

Paux, J., Morin, L., Brenner, R., and Kondo, D. (2015).
An approximate yield criterion for porous single crystals.
Eur. J. Mech./A, 51 :1–10.

Rice, J. (1976).

The localisation of plastic deformation.
In Koiter, W., editor, *Proc. 14th Int. Conf. Theoretical and Applied Mechanics, Delft*, pages 207–220. North–Holland, Amsterdam.

Rice, J. (1980).
The mechanics of earthquake rupture. Proceedings of the international school of physics "Enrico Fermi", pages 555–649.
North-Holland.

Rice, J. R. and Tracey, D. M. (1969).
On the ductile enlargement of voids in triaxial stress fields.
J. Mech. Phys. Solids, 17 :201–217.

Rivalin, F., Besson, J., Pineau, A., and Di Fant, M. (2000).
Ductile tearing of pipeline-steel wide plates — II. : Modeling of in–plane crack propagation.
Eng. Fract. Mech., 68(3) :347–364.

Rudnicki, J. and Rice, J. (1975).
Conditions for the localization of deformation in pressure–sensitive dilatant materials.
J. Mech. Phys. Solids, 23 :371–394.

Ruggieri, C., Panontin, T., and Dodds Jr., R. H. (1996).
Numerical modeling of ductile crack growth in 3-d using computational cell elements.
Int. J. Frac., 82 :67–95.

Shakoor, M., Bernacki, M., and Bouchard, P. (2018).

Ductile fracture of a metal matrix composite studied using 3d numerical modeling of void nucleation and coalescence.
Eng. Fract. Mech., 189 :110–132.

Shinohara, Y., Madi, Y., and Besson, J. (2016).
Anisotropic ductile failure of a high-strength line pipe steel.
Int. J. Frac., 197 :127–145.

Soret, C., Madi, Y., Gaffard, V., and Besson, J. (2017).
Local approach to fracture applied to the analysis of a full size test on a pipe containing a girth weld defect.
Eng. Fail. Anal., 82 :404–419.

Tanguy, B., Besson, J., Piques, R., and Pineau, A. (2005).
Ductile—brittle transition of a A508 steel characterized by the Charpy impact test. Part—II : modelling of the Charpy transition curve.
Eng. Fract. Mech., 72 :413–434.

Tanguy, B., Luu, T., Perrin, G., Pineau, A., and Besson, J. (2008).
Plastic and damage behavior of a high strength X100 pipeline steel : experiments and modelling.
Int. J. of Pressure Vessels and Piping, 85(5) :322–335.

Thomason, P. F. (1985a).
A three–dimensional model for ductile fracture by the growth and coalescence of microvoids.
Acta Metall., 33(6) :1087–1095.

Thomason, P. F. (1985b).
Three–dimensional models for the plastic limit–loads at incipient failure of the intervoid matrix in ductile porous solids.
Acta Metall., 33(6) :1079–1085.

Torki, M., Benzerga, A., and Leblond, J.-B. (2015).
On void coalescence under combined tension and shear.
J. Applied Mech., 82.

Tvergaard, V. and Needleman, A. (1984).
Analysis of the cup–cone fracture in a round tensile bar.
Acta Metall., 32 :157–169.

Xia, L. and Shih, C. F. (1995).
Ductile crack growth — I. A numerical study using computational cells with microstructurally-based length scales.
J. Mech. Phys. Solids, 43 :233–259.

Xia, L., Shih, C. F., and Hutchinson, J. W. (1995).
A computational approach to ductile crack growth under large scale yielding conditions.
J. Mech. Phys. Solids, 43(3) :389–413.

Zhang, Y., Lorentz, E., and Besson, J. (2018).
Ductile damage modelling with locking-free regularised gtn model.
Int. J. Numer. Meth. Engng, 113(13) :1871–1903.

Zhang, Z., Thaulow, C., and Ødegård, J. (2000).
A complete Gurson model approach for ductile fracture.
Eng. Fract. Mech., 67(2) :155–168.

MINES ParisTech

CENTRE DES MATERIAUX
P.M FOURT

www.mat.mines-paristech.fr